



Synthesis and bioevaluation of *N*-(3,4,5-trimethoxyphenyl)-1*H*-pyrazolo [3,4-*b*]pyridin-3-amines as tubulin polymerization inhibitors with anti-angiogenic effects

Shu-Yi Hao¹, Zhi-Yuan Qi¹, Shuai Wang, Xing-Rong Wang, Shi-Wu Chen^{*}

School of Pharmacy, Lanzhou University, Lanzhou 730000, China

ARTICLE INFO

Keywords:

Aniogenesis
Tubulin polymerization
Inhibitors
Pyrazolo[3,4-*b*]pyridine
Antitumor

ABSTRACT

A new series of *N*-(3,4,5-trimethoxyphenyl)-1*H*-pyrazolo[3,4-*b*]pyridin-3-amine derivatives as tubulin polymerization inhibitors were synthesized, and evaluated for the anti-proliferative activities. A structure–activity relationship study revealed that the free amino moiety of 1*H*-pyrazolo[3,4-*b*]pyridin-3-amine played an essential role in the anti-proliferative activities. Especially, compound **15c** displayed the strongest anti-proliferation against MCF-7 cells with IC₅₀ value of 0.067 ± 0.003 μM, and high selectivity over the normal human embryonic lung WI-38 cells with IC₅₀ value of 23.41 ± 1.53 μM. Further mechanistic studies revealed that **15c** showed strong anti-tubulin polymerization activity, changed the morphology of tubulin, and arrested the cell cycle at the G2/M transition in MCF-7 cells. Molecular docking analysis suggested that **15c** well occupied the colchicine-binding pocket of tubulin. Additionally, **15c** demonstrated anti-angiogenic activities with blocking the migration, invasion and tube formation, disrupting the newly formed tube, and regulating both MMP-9 and TIMP-1 in HUVEC cells. In summary, our results highlight that compound **15c** is a potential antitumor compound that are worthy of further development.

1. Introduction

Microtubules are a key component of the cytoskeleton and are present in almost all eukaryotic cells except for a few types such as human red blood cells.¹ They consist of globular proteins composed of α- and β-tubulin heterodimers, and they play key roles in cellular processes such as organellar movement, intracellular transport, the formation and maintenance of cell shape, and cell division.² On the other hand, the inhibition of tubulin assembly into microtubules, or, inversely, the depolymerization of microtubules, leads to the arrest of cell division and eventually to apoptosis.³ This makes microtubule-targeting agents (MTAs) are an effective and attractive molecular target for cancer chemotherapeutics.⁴ Current MTAs include the colchicine, vinca alkaloids, and taxanes sites with the first two binding to the so-called colchicine- and vinca-binding sites and acting as tubulin polymerization destabilizers, whereas the latter bind to the taxanes-binding site and act as polymerization stabilizers.⁵ These MTAs can interfere with the microtubule equilibrium process, and the success of tubulin polymerization inhibitors as anticancer agents has stimulated significant interest in the

identification of new compounds that may be more potent or more selective in targeting tissues or tumors.⁶

Combretastatin-A4 (CA-4, **1**, Fig. 1) is a natural *cis*-stilbene product isolated from the bark of the African willow tree, *Combretum caffrum*, and it is a well-known molecule that strongly inhibits tubulin polymerization by binding to the colchicine-binding site, causing rapid vascular shutdown and cell death in tumor cells.⁷ However, the poor water solubility and bioavailability of CA-4 have hindered its development into an antitumor drug.⁸ To overcome these shortcomings, its water-soluble ester, CA-4P, was developed as a tumor vascular-targeting agent and entered into clinical trials for the treatment of platinum-resistant ovarian cancer.⁹ Unfortunately, the study was terminated owing to a lack of efficacy in improving progression-free survival, combined with an unfavorable objective response rate.¹⁰

Due to its important pharmacological characteristics and simple structure, a wide variety of CA-4 analogs have been developed and evaluated in structure-activity (SAR) studies.^{11–16} These studies showed that the 3,4,5-trimethoxyphenyl (TMP) moiety (A ring) is an important pharmacodynamic point for tubulin binding, and the oxygen atom of its

^{*} Corresponding author.

E-mail address: chenshw@lzu.edu.cn (S.-W. Chen).

¹ These authors made equal contributions to this work.

4-methoxy group interacts with the Cys241 residue at the colchicine-binding site.^{17,18} While the B ring can be replaced with a various heterocycle, such as benzofuran, benzothiophene, and indole, among others, the resulting compounds retain their tubulin polymerization inhibitory activity.^{5,11} Thus the modification of the B ring has become the focus of research, and some derivatives with superior antitumor activities were found. For example, isoazaerianin (3), in which the *cis*-stilbene was substituted with methylamino, displays anti-cancer activities with nanomolar IC₅₀ cytotoxicity against a panel of cancer cells and inhibits tubulin assembly at a micromolar level.¹⁹ Further, compound 4 with benzofuran showed good proliferation inhibitory activity against the HeLa, A549, HT-29, MCF-7, and HL-60 cell lines, with IC₅₀ values in the range of 13–24 nM.²⁰ In addition, the Tung group synthesized compound 5 with a 1*H*-indazole and found that its IC₅₀ toward KB cells was 20 nM.²¹

Hybrid molecules have the potential to enhance efficacy, overcome drug resistance, and reduce toxicity, and several hybrid molecules have been subjected to clinical evaluations for the treatment of various diseases.²² We previously described a series of 1-(benzofuran-3-yl)-4-(3,4,5-trimethoxyphenyl)-1*H*-1,2,3-triazole derivatives as tubulin polymerization inhibitors with marked cytotoxicity.²³ As part of our ongoing search for novel tubulin polymerization inhibitors based on CA-4, we designed and synthesized a series of *N*-(3,4,5-trimethoxyphenyl)-1*H*-pyrazolo[3,4-*b*]pyridin-3-amine derivatives that are hybrids of compounds 4 and 5 and further modified using bioisosteric replacement of the benzene moiety with pyridine (Fig. 2). Herein, we report the synthesis and structure-activity relationship of a set of novel target compounds 14–15. Furthermore, we present the biological activities of a representative compound 15c, including their effects on *in vitro* tubulin polymerization, intracellular microtubule networks, cell cycle transition, as well as anti-angiogenic effects in HUVEC cells. In addition, molecular modeling analysis of the colchicine-binding site of tubulin was performed with 15c.

2. Results and discussion

2.1. Chemistry

The synthetic route to the target compounds is outlined in Scheme 1. Initially, the substitution of 2-chloro-6-methoxypyridine as the starting material with *N*-bromosuccinimide (NBS) in the presence of benzoyl peroxide (BPO) yielded 3-bromo-2-chloro-6-methoxypyridine (9), and the Bouveault reaction of 9 provided 2-chloro-6-methoxynicotinylaldehyde (10), which reacted with hydrazine hydrate under refluxing conditions produced 6-methoxy-1*H*-pyrazolo[3,4-*b*]pyridine (11). Subsequent bromination of 11 at the 3-position with NBS generated 3-bromo-6-methoxy-1*H*-pyrazolo[3,4-*b*]pyridine (12), and substitution of the latter with different haloalkanes in the presence of NaH in dimethylformamide (DMF) afforded *N*¹-substituted pyridopyrazole derivatives 13a–e, while protection with 3,4-dihydro-2*H*-pyran in the presence of *p*-toluenesulfonic acid in tetrahydrofuran (THF) yielded 13f. Next, Buchwald-Hartwig coupling of 13a–f with 3,4,5-trimethoxyaniline catalyzed by Pd(OAc)₂ provided the compounds 14a–f.

Compounds 14a,b were further reacted with corresponding haloalkane under NaH in DMF to obtain the target compounds 15a,b, respectively. Simultaneously, reaction of compounds 14e,f with various haloalkane, and further deprotection yielded the target compounds 15c–i. All target derivatives were fully characterized by ¹H NMR, ¹³C NMR, and HRMS spectroscopic techniques, and their purities were more than 95% based on HPLC analysis. The spectral data were in full agreement with the expected structures (see Experimental Section and Supporting Information).

2.2. Biological evaluation

2.2.1. Anti-proliferative activities of target compounds 14a–d, 15a–l

Target compounds 14a–d and 15a–l were evaluated for the anti-proliferative activity against five human cancer cell lines (HCT116, colon cancer; A549, non-small-cell lung cancer; HeLa, human epithelial cervical cancer; MCF-7, human breast cancer; and HepG2, hepatic carcinoma) and the WI-38 cell line (normal human embryonic lung cells) using the MTT assay with CA-4 as the reference drug.²⁴ The IC₅₀ values of the compounds are summarized in Table 1.

Compounds 14a–d and 15a,b, in which the amino of 1*H*-pyrazolo [3,4-*b*]pyridine at *N*¹ was substituted with various R₁, generally showed poor proliferation inhibitory activity against the five human cancer cell lines. Encouragingly, compounds 15c–l with a free amino group at *N*¹ of the 1*H*-pyrazolo[3,4-*b*]pyridine had dramatically improved anti-proliferative activities. In addition, the introduction of CH₂CH₂F at the bridge connection improved this anti-proliferative activity (15 g vs 15d), while the activities of 15 h, in which the amino of 1*H*-pyrazolo [3,4-*b*]pyridine was substituted with CH₂CHF₂, were superior compared with those of unsubstituted 15d, and weaker than those of 15g. In particular, compounds 15c and 15g showed not only superior anti-tumor activities but also low toxicities, as the IC₅₀ of compound 15c against MCF-7 cells was 0.067 ± 0.003 μM and 23.41 ± 1.53 μM against WI-38 cells, while the IC₅₀ of 15g against HeLa cells was 0.012 ± 0.009 μM and 16.48 ± 1.60 μM against WI-38 cells. These SAR studies showed that derivatives with an unsubstituted 1*H*-pyrazolopyridine ring displayed better activity profiles, and when the NH at the connection was substituted with a small group, this activity improved.

2.2.2. *In vitro* tubulin polymerization inhibition activities of 15c and 15g

Mechanistic researches have revealed that the potent anticancer activity of CA-4 is based on its inhibition of tubulin polymerization.⁸ To elucidate whether 15c and 15g also target the tubulin-microtubule system, the *in vitro* tubulin polymerization inhibitory activities of 15c and 15g were evaluated using the method previously described.²³ As shown in Fig. 3, after tubulin was incubated with 15c and 15g at various concentrations, the absorbance values decreased compared with the control. These results indicated that 15c and 15g both inhibited tubulin polymerization *in vitro* and that this inhibition occurred in a concentration-dependent manner, with IC₅₀ values of 14.0 ± 3.3 μM and 55.7 ± 2.0 μM respectively. Moreover, 15c showed stronger inhibition of tubulin polymerization than that of 15g, although weaker than CA-4 (1.8 ± 0.1 μM). Considering compound 15c possessed more potent anti-

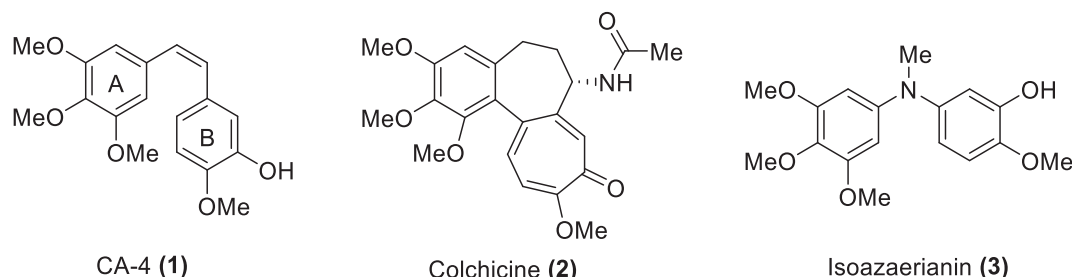


Fig. 1. Structures of CA-4 (1), colchicine (2) and isoazaerianin (3).

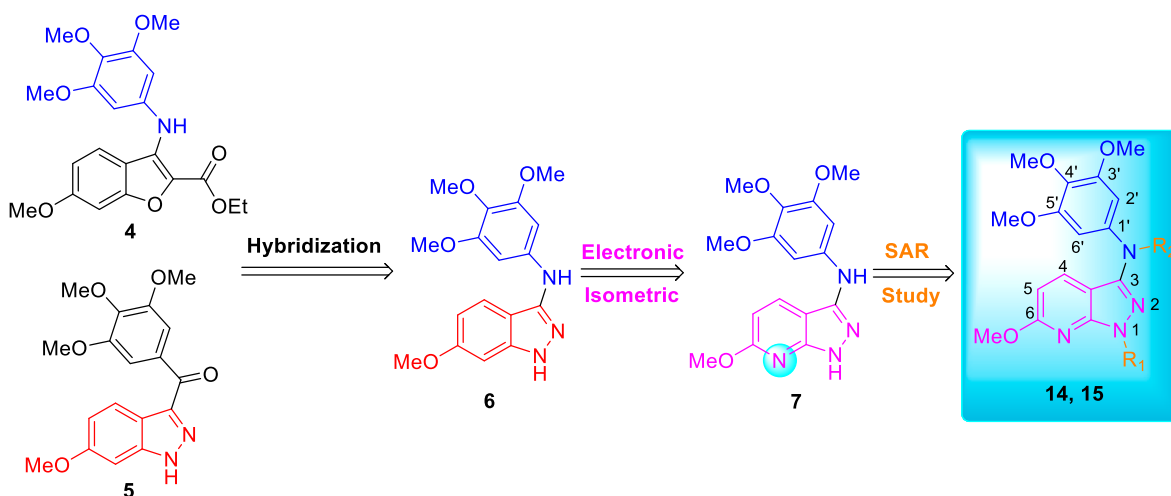
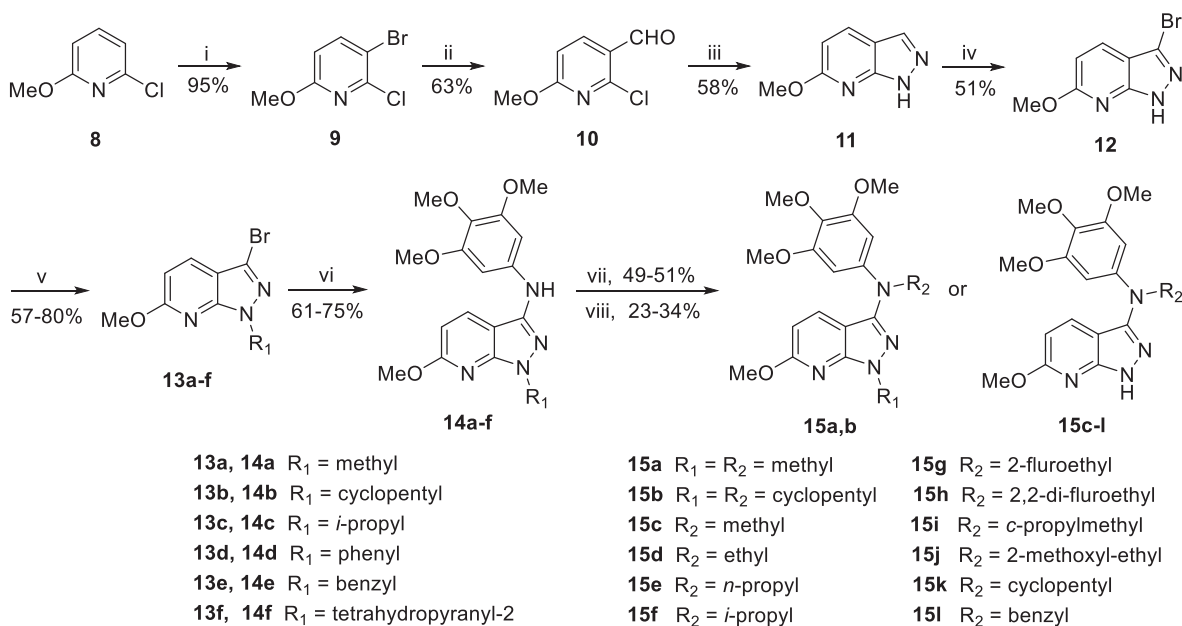


Fig. 2. Design of target compounds.



Scheme 1. Reagents and conditions: (i) NBS, BPO, CH₃CN, 90 °C, 3 h; (ii) DMF, *n*-BuLi, dry THF, -78 °C, 1.5 h; rt, 6 h; (iii) N₂H₄·H₂O, H₂O, reflux, 5 h; (iv) NBS, CH₂Cl₂, -30 °C, 30 min; (v) haloalkane (for **13a–e**), NaH, DMF, rt, 24 h; or *p*-TsOH, 3,4-dihydro-2H-pyran (for **13f**), THF, 80 °C, 3 h; (vi) 3,4,5-trimethoxyaniline, xantphos, Pd(OAc)₂, Cs₂CO₃, dioxane, reflux, 3 h; (vii) **14a** and MeI (for **15a**), or **14b** and cyclopentylchloride (for **15b**), NaH, DMF, rt, 24 h; (viii) **14e,f**, haloalkane, NaH, DMF, rt, 24 h; then HCl/EtOH, rt, 2–12 h (for **15c–l**).

tubulin polymerization and less toxicity against WI-38 normal cells than those of **15g**. Therefore, compound **15c** was chosen to further study of its biological activity and action mechanisms.

2.2.3. Docking study

CA-4 has good anti-tubulin polymerization activity because it can bind to the colchicine-binding site, thereby inhibiting the polymerization of tubulin.¹⁵ As our above experiments showed, compound **15c** showed good anti-tubulin polymerization activity. In order to identify that **15c** inhibits microtubule polymerization by binding to colchicine site instead of vincristine, we used Schrödinger software for molecular docking simulations at the colchicine and vincristine sites of tubulin (PDB code: 1Z2B).^{17,25} As shown in Fig. 4A, the TMP ring of **15c** is embedded in the β₂-tubulin end, and the pyrazolopyridine ring is located toward the GTP end. Furthermore, **15c** has almost the same spatial conformation with CA-4, and the N¹H of pyrazolopyridine forms stable hydrogen bonding with Thr179, which further enhances the

affinity with β₂-tubulin. In addition, the TMP ring can go deep into the binding pocket composed of Ala250, Leu242, Cys241, Val238, and Ile378. Among these residues, the mercapto group in the Cys241 is very close to the 4'-OMe of **15c**, which shows a certain interaction force (Fig. 4C). From Fig. 4B, it can be found that the vincristine binding site of **15c** exists on α₂-tubulin and is adjacent to GDP end in β₁-tubulin. However, **15c** does not penetrate into the binding pocket of vincristine, and fails to form hydrogen bonds and hydrophobic interactions with key amino acid residues in the pocket, such as Asn329, Pro175, Val177, Ser178, Pro325 and Val353 (Fig. 4D). Therefore, the docking simulations indicated that compound **15c**, like CA-4, is a tubulin destabilizer that binds to the colchicine site.

2.2.4. Effect of **15c** on microtubule organization

Since tubulin plays a vital role in maintaining cell shape and basic cell function, we used immunofluorescence to investigate whether **15c** could disrupt microtubule dynamics in living cells (MCF-7 cells). As

Table 1
Anti-proliferative activities of compounds **14a–d** and **15a–l**.

Comps	IC ₅₀ (μM) ^{a,b}					
	HCT-116	A549	HeLa	MCF-7	HepG2	WI-38
14a	>50	>50	6.07 ± 0.43	>50	6.24 ± 0.13	2.43 ± 0.81
14b	>50	>50	6.28 ± 1.03	22.35 ± 1.18	>50	73.83 ± 3.71
14c	12.00 ± 4.49	31.86 ± 3.34	12.85 ± 2.58	13.24 ± 2.69	20.04 ± 0.57	4.32 ± 0.67
14d	>50	>50	22.50 ± 3.01	>50	38.84 ± 7.46	12.56 ± 4.48
15a	>50	>50	0.59 ± 0.26	>50	2.52 ± 0.32	22.80 ± 2.94
15b	>50	>50	>50	>50	>50	138.43 ± 6.95
15c	0.26 ± 0.02	6.00 ± 2.24	0.21 ± 0.04	0.067 ± 0.003	4.79 ± 1.56	23.41 ± 1.53
15d	16.67 ± 7.25	31.17 ± 7.49	0.70 ± 0.13	0.81 ± 0.15	9.64 ± 3.79	8.03 ± 1.25
15e	5.97 ± 1.38	>50	0.73 ± 0.02	1.37 ± 0.78	6.26 ± 0.88	2.99 ± 1.76
15f	>50	>50	21.17 ± 2.02	>50	24.46 ± 2.26	6.04 ± 0.76
15g	0.12 ± 0.03	0.20 ± 0.08	0.012 ± 0.009	0.102 ± 0.012	5.79 ± 0.56	16.48 ± 1.60
15h	0.47 ± 0.14	2.42 ± 0.52	0.17 ± 0.02	21.73 ± 3.28	18.75 ± 2.34	1.69 ± 0.26
15i	2.18 ± 0.55	20.56 ± 2.54	0.18 ± 0.04	2.35 ± 0.93	5.46 ± 1.49	1.29 ± 0.11
15j	3.66 ± 0.88	31.77 ± 9.04	1.77 ± 0.37	1.72 ± 0.69	>50	30.85 ± 2.47
15k	26.23 ± 2.11	22.71 ± 8.38	28.43 ± 4.67	>50	>50	10.41 ± 6.03
15l	3.37 ± 0.31	>50	3.19 ± 1.04	10.35 ± 1.97	7.38 ± 0.72	1.67 ± 0.01
CA-4	0.029 ± 0.005	0.058 ± 0.004	0.005 ± 0.002	0.034 ± 0.008	0.28 ± 0.13	31.57 ± 6.06

^a IC₅₀ values are presented as the means ± SD of triplicate experiments.

^b Drug treatment for 72 h.

shown in Fig. 5, in the control group, the microtubule network showed normal arrangement and organization. However, after the addition of **15c**, the spindle formation showed obvious abnormalities and breakage. When the concentration of compound **15c** was 10 nM, the microtubules gradually began to shrink around the nucleus. When the concentration increased to 100 nM, the microtubule spindle showed clear shrinkage around the center of the cell, forming a clump. The morphological microtubule changes indicated that compound **15c** dramatically disrupted the microtubule organization in a concentration-dependent manner, and such changes may eventually lead to cell cycle disruption.

2.2.5. Effect of **15c** on cell cycle

Since most tubulin destabilizers can disrupt regulated cell cycle distribution, we chose flow cytometry to detect whether **15c** was able to block the cell cycle.²⁶ As shown in Fig. 6A, after the addition of 5 nM and 10 nM **15c**, the G2/M population increased from 16.81% (control) to 63.50% and 80.73%, respectively. The results indicate that compounds **15c** can block cancer cells in the G2/M phase. However, compound **15c** did not induce apoptosis of MCF-7 cells like others CA-4 derivatives as tubulin polymerization inhibitors (Fig. S1).

To further validate these findings, we used western blot analysis to detect the effect of compounds **15c** on the cyclins Cdc25c, Cdc2, and Cyclin B1 at the protein level. It is known that the activation of Cdc2 kinase is controlled by Cyclin B1 binding and that Cdc25c phosphorylation can promote the mitosis of eukaryotic cells, leading to cell division.²⁷ As shown in Fig. 6B, compared with the control group, the protein levels of Cdc25c, Cdc2, and Cyclin B1 were significantly reduced following treatment with **15c** at 10 nM, 50 nM and 100 nM. From densitometry analysis of these western blots (Fig. 6C), it can be seen that the expression of these proteins showed a concentration-dependent decrease with increasing compound concentration. The results suggest that compound **15c** arrest MCF-7 cells in the G2/M transition by reducing the levels of Cdc25c, Cdc2, and Cyclin B1.

2.2.6. Effect of **15c** on VEGF-A in MCF-7 cells

Vascular endothelial growth factor (VEGF) can be secreted by tumor cells and subsequently promote HUVECs growth in Ischemic area of

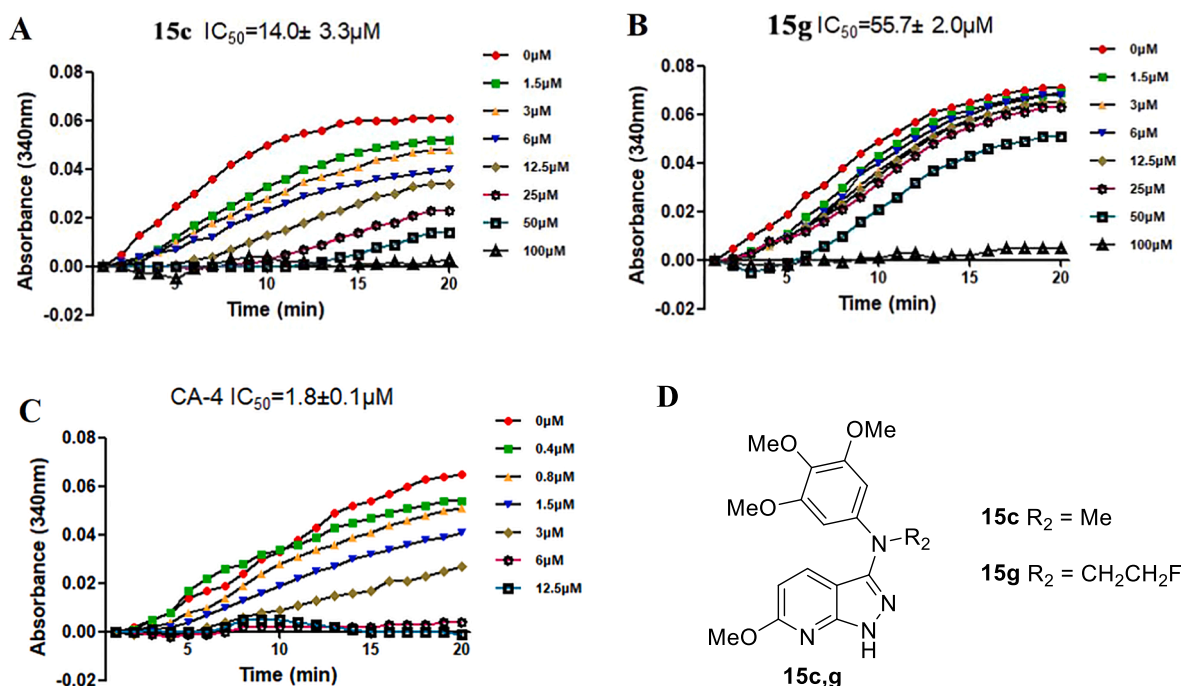


Fig. 3. Tubulin polymerization inhibitory activities of **15c**, **15g** and CA-4. Purified tubulin protein at 10 μM was incubated at 37 °C in the absence or presence of **15c** (A), **15g** (B) and CA-4 (C) at the indicated concentrations; (D) Chemical structures of **15c** and **15g**.

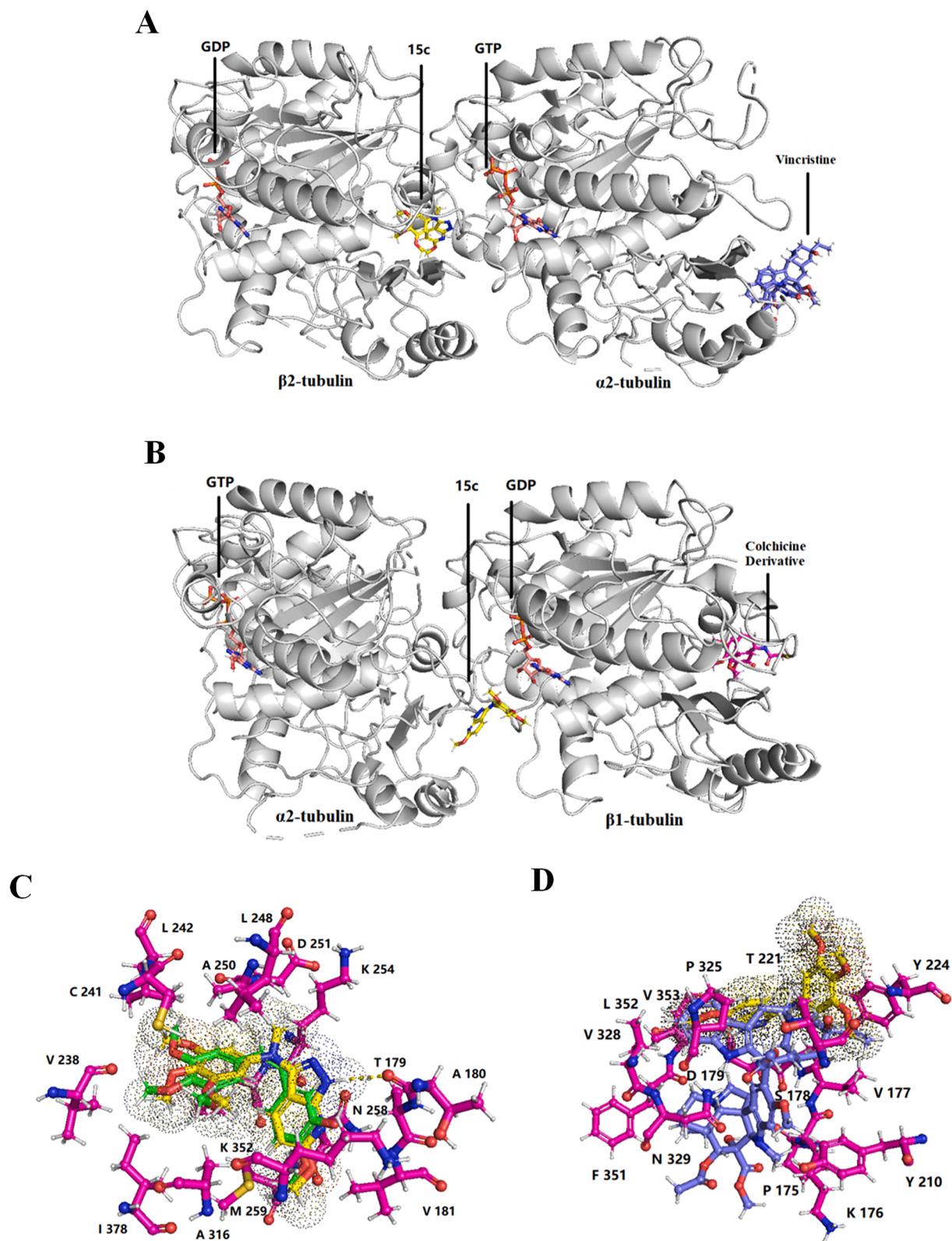


Fig. 4. Molecular docking of 15c at different binding site of the tubulin (PDB code: 1Z2B). (A) Surface representation of 15c at colchicine binding site. (B) Surface representation of 15c at vincristine binding site. (C) The interaction of 15c (yellow sticks) with surrounding amino acid residues (pink sticks) of β 2-tubulin compared with CA-4 (green). (D) The interaction of 15c (yellow sticks) with surrounding amino acid residues (pink sticks) of α 2-tubulin compared with vincristine (purple). (For interpretation of the references to colour in this figure legend, the reader is referred to the web version of this article.)

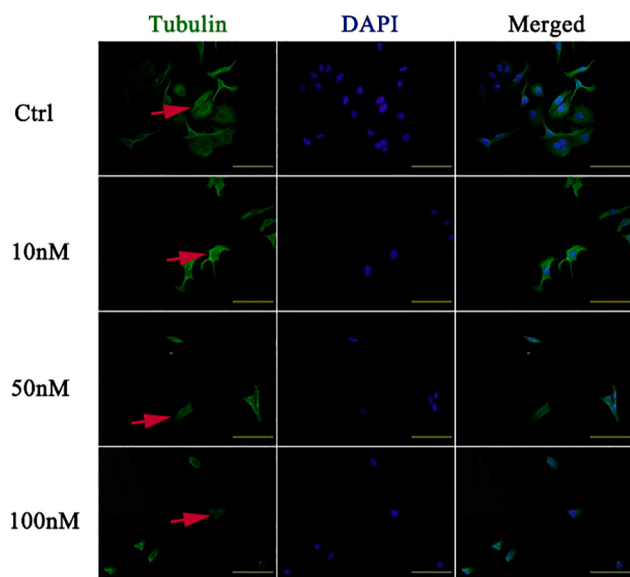


Fig. 5. Effect of **15c** on microtubule organization of MCF-7 cells. MCF-7 cells were plated in confocal dishes and incubated with **15c** at indicated concentrations for 6 h. The images were observed and photographed with a laser scanning confocal microscope. Scale bar: 100 μ m.

tumor tissues to draw adequate nutrition, and the VEGF-A is considered to be one of the important regulators of angiogenesis.²⁸ Therefore, reducing the expression of VEGF-A in tumor tissues plays a vital role in tumor angiogenesis. Thus, we tested the effects of **15c** on VEGF-A in MCF-7 cells, and found a apposite decrease in VEGF-A expression in the group with high-concentration **15c** treatment (Fig. 7). The result revealed that **15c** has a significant effect on angiogenesis in tumor

tissue, leading to “starvation” of the tumor.

2.2.7. Effects of **15c** on HUVEC cells migration and invasion

The migration and invasion of HUVEC plays an important role in the early stage of tumor angiogenesis.²⁹ The IC_{50} value of **15c** against HUVEC cells was $23.5 \pm 1.80 \mu$ M in MTT method, thus we chose HUVEC cell cultures to evaluate the ability of compound **15c** (from 0.1 to 1 μ M) to inhibit HUVEC cell migration and invasion.³⁰ As shown in Fig. 8A, after 24 h the control group showed complete coverage of the scratches due to the migration of the HUVEC cells. In contrast, treatment with **15c** at any of the tested concentrations prevented the migration of the HUVEC cells. Compared with the 100% migration rate of the control group at 24 h, the cell migration rates following treatment with compound **15c** at 0.1 μ M, 0.5 μ M, and 1 μ M were 26.4%, 26.6%, and 22.4%, respectively (Fig. 8B). From these results, it can be concluded that compound **15c** can inhibit the migration of HUVEC cells. Similarly, the results from the transwell chamber revealed that **15c** could significantly suppress the invasion ability of HUVECs in a dose-dependent manner (Fig. 8C and 8D). The above results are consistent with previous findings that CA-4 has an inhibitory effect on the angiogenesis.³¹

Matrix metalloproteinases (MMPs), in particularly MMP-9, play critical roles in remodeling the extracellular matrix (ECM) by digesting various ECM proteins in the basement membrane.³² Through their MMP-inhibitory activities, tissue inhibitors of metalloproteinases (TIMPs) such as TIMP-1 are capable of inhibiting tumor invasion and metastasis in experimental cancer models.³³ Next, we used western blotting to measure expression levels of MMP-9 and TIMP-1 in HUVEC cells exposed to various concentrations of **15c** for 24 h.³² Western blotting revealed that decreased levels of MMP-9, and increased levels of TIMP-1 in HUVEC cells following exposure to **15c** (Fig. 9). These findings suggest that **15c** presumably inhibit migration and invasion of HUVEC cells by down-regulation the activity of MMP-9 and up-regulation TIMP-1.

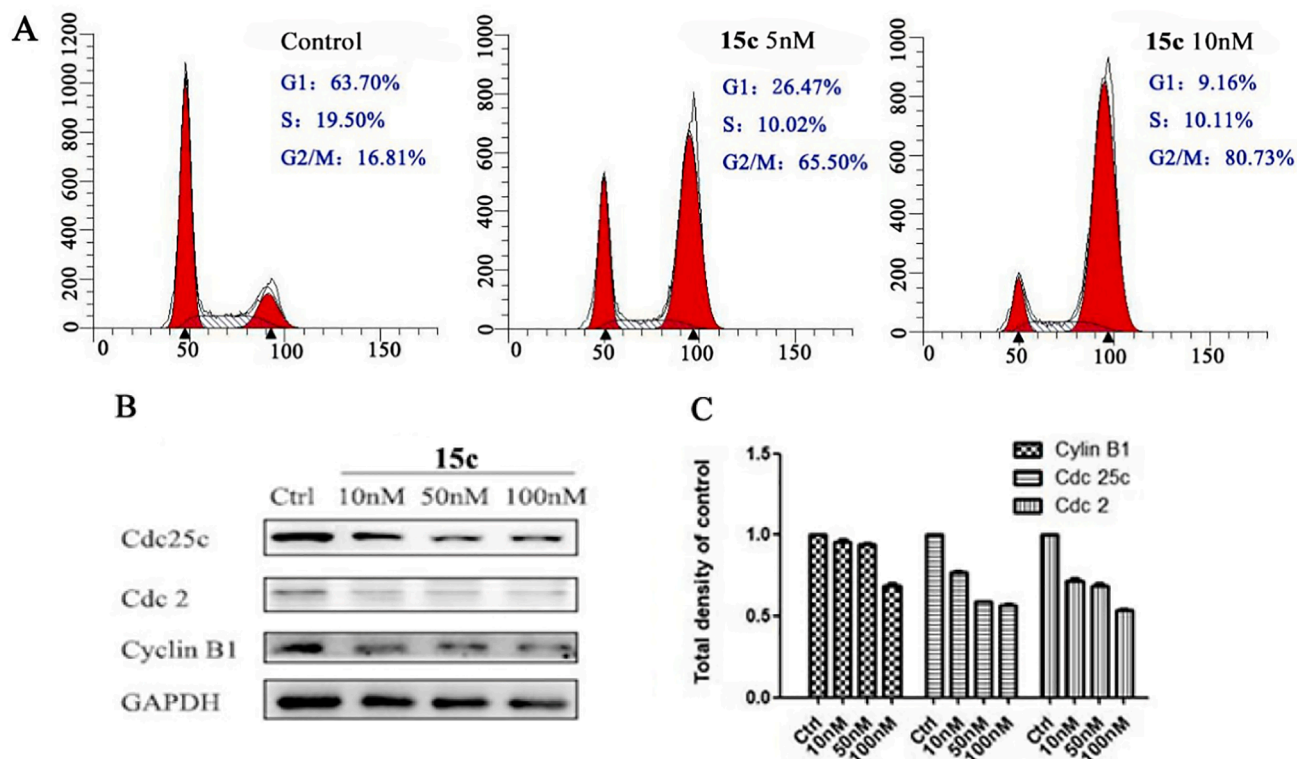


Fig. 6. Effect of compound **15c** on cell cycle. (A) MCF-7 cells were treated with 0, 5 and 10 nM **15c** for 24 h, and detected by flow cytometry. (B) MCF-7 cells were treated with 0, 10, 50 and 100 nM **15c** for 24 h, and the level of Cdc25c, Cdc2 and Cyclin B1 were tested by west blotting. (C) The histogram of **15c** on cycle-related proteins Cdc25c, Cdc2 and Cyclin B1 in average of two independent experiments.

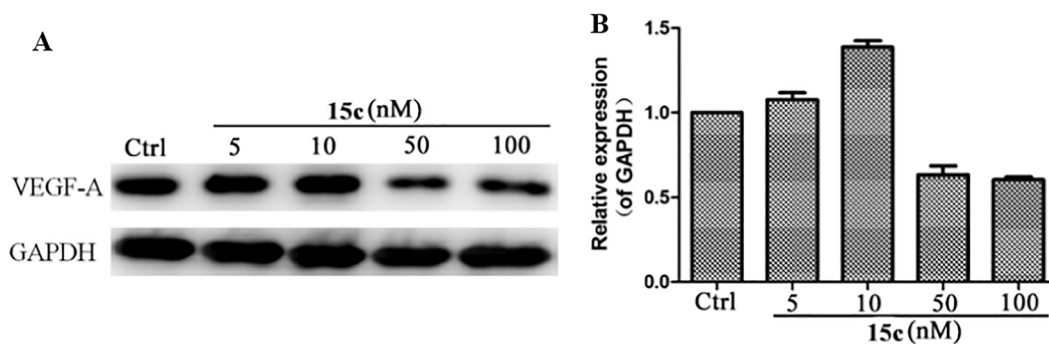


Fig. 7. Effect of compound **15c** on VEGF-A in MCF-7 cells. (A) MCF-7 cells were treated with **15c** at various concentrations for 24 h. (B) quantitative analysis of the VEGF-A protein expression, result are showed as mean \pm SD of three independent experiments.

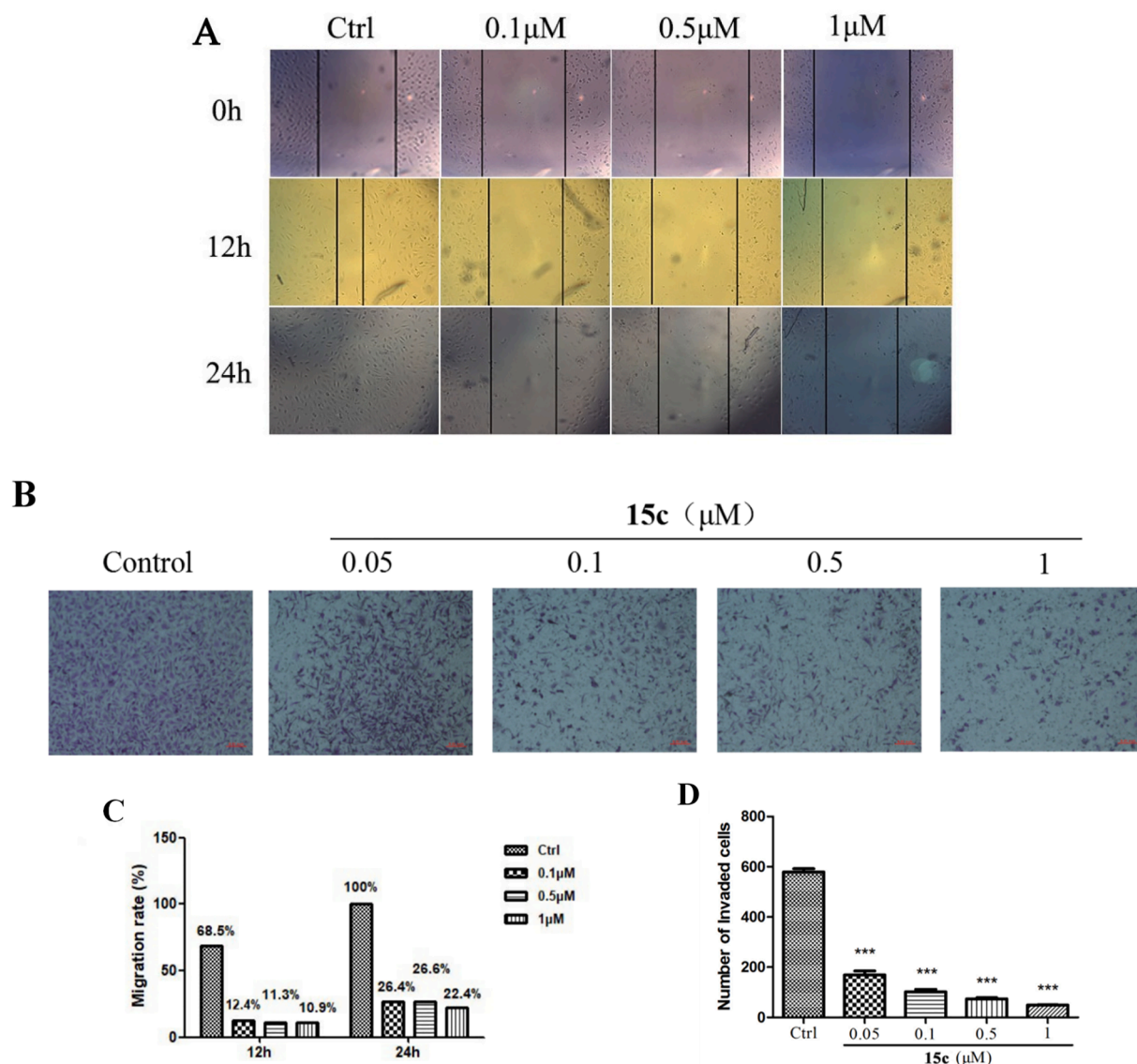


Fig. 8. Effects of **15c** on migration and invasion in HUVEC cells. (A) HUVEC cells treated with **15c** at indicated concentrations for 12 and 24 h, and the number of relative closure of scratches in wound healing assay; (C) HUVEC cells were treated with **15c** at indicated concentrations for 24 h, and the number of invaded cells in transwell invasion assay. The statistical histogram of the effects of **15c** on migration (B) and invasion (D) of HUVEC cells. *** $P < 0.001$. Data are presented as mean \pm SD of three independent experiments.

2.2.8. Effect of **15c** on tube formation of HUVEC cells

In the late stage of angiogenesis, endothelial cells have completed the steps of proliferation and migration and are arranged to form a long

lumen-like structure.³⁴ We, therefore, evaluated the anti-vascular activity of compound **15c** based on HUVEC tubule formation (Fig. 10). The control group formed an extensive network lumen-like structure, and

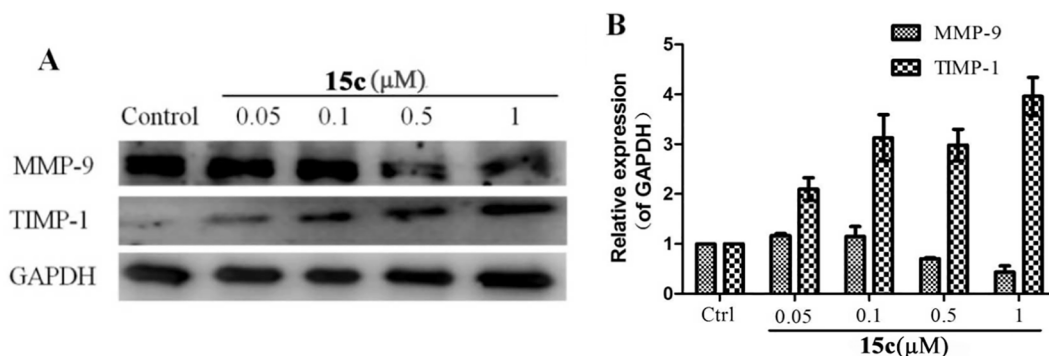


Fig. 9. The effects of **15c** on expression of MMP-9 and TIMP-1 in HUVECs. (A) Analysis of expression of MMP-9 and TIMP-1 in HUVECs exposed to 0, 0.05, 0.1, 0.5 μM and 1 μM **15c** for 24 h by western blotting. (B) Quantitative level of proteins in HUVECs after **15c** treatment. All data were expressed as the mean ± SD of three independent experiments.

the small tubes were tightly connected. When **15c** was added at a concentration of 0.1 μM, tubule formation was inhibited, and as the concentration increased, the inhibitory effect on tubule formation became more obvious. When the concentration of **15c** was 1 μM, the formation of HUVEC cell tubules was almost completely inhibited. These results showed that compound **15c** can inhibit HUVEC cell tubule formation in a dose-dependent manner, thereby effectively inhibiting angiogenesis.

2.2.9. Effect of **15c** on disruption of newly formed vascular structures of HUVEC cells

Since microtubule disruption is a major aspect of the antivascular activity of CA-4 and its prodrug CA-4-phosphate,³⁵ so we investigated whether **15c** displayed vascular targeting effects *in vitro* models by disrupting the formed tube-like structures. *In vitro*, HUVECs seeded on a permissive thick layer of the reconstituted basement membrane, matrigel rapidly aligned and formed a network of cords, which is reminiscent of newly formed vessels after 6 h. The addition of **15c** (0, 0.1, 0.5 or 1 μM) to these newly formed tube-like structures, after incubation for 6 h, photographs were taken. As showed in Fig. 11, **15c** disrupts the integrity of the network in a dose-dependent manner. Taken together, these data indicated that **15c** displayed not only tubule formation-inhibiting activity, but also vascular-disrupting activity.

3. Conclusion

In summary, we designed and synthesized a series of novel pyrazolopyridine tubulin polymerization inhibitors using hybrid approach. After preliminary biological activity evaluation and mechanism research, we found compound **15c** displayed better anti-proliferation on tumor cells and weak toxicity to normal cells WI-38. Furthermore, **15c** showed strong anti-tubulin polymerization activity, and changed the intracellular tubulin morphology, and formed similar combination mode to CA-4 and better hydrophobic effect at the colchicine site, indicating that it can inhibit microtubules by binding to the colchicine

site rather than vincristine site. By reducing the expression of cyclin Cdc 2, Cdc25c and Cyclin B1, **15c** arrested tumor cells in the G2/M phase. In addition, **15c** played an anti-angiogenic role by blocking tubule formation and inhibiting migration and invasion of HUVEC cells. Studies have shown that compound **15c** as an effective tubulin polymerization inhibitor is worthy of subsequent *in vivo* pharmacokinetic experiments and evaluation of *in vivo* antitumor experiments.

4. Experimental protocols

4.1. Chemistry

All starting materials and reagents were purchased commercially and used without further purified, unless otherwise stated. All reactions were monitored by thin layer chromatograph (TLC) on silica gel GF₂₅₄ (0.25 mm thick). Column chromatography (CC) was performed on Silica Gel 60 (230–400 mesh, Qingdao Ocean Chemical Ltd., China). HPLC analysis using a UltiMate300 DAD HPLC system equipped with a PU-2089 Plus quaternary gradient pump and a UV-2075 Plus UV-vis detector, using an Alltech Kromasil C18 column with dimensions of 250 mm × 4.6 mm and 5 μm particle size. ¹H NMR and ¹³C NMR spectrum were recorded on an Agilent NMR inova 600 spectrometer with TMS as an internal standard, all chemical shift values were reported as ppm. Mass spectra were recorded on an Esquire 6000 (ESI-ION TRAP) spectrometer or LTQ-Orbitrap-ETD (Thermo Scientific, USA) with ESI source as ionization, respectively.

4.1.1. 3-Bromo-2-chloro-6-methoxyppyridine (**9**)

To a solution of 2-chloro-6-methoxyppyridine (**8**) (30.00 g, 209.0 mmol) and dibenzoyl peroxide (BPO) (2.53 g, 10.4 mmol) in acetonitrile (120 mL), *N*-bromosuccinimide (55.79 g, 313.4 mmol) was slowly added in small portions at room temperature followed by further refluxing for 3 h. After the reaction was completed, the solution was cooled and concentrated under reduced pressure. The residue was dissolved with

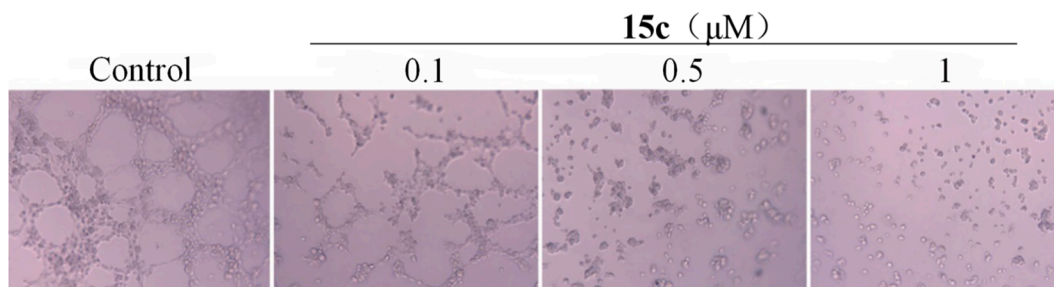


Fig. 10. Effects of **15c** on the formation of HUVEC cell tubules. HUVEC cells were seeded with **15c** at concentration of 0, 0.1, 0.5 and 1 μM for 6 h on matrigel coated plates, and the representative images of preformed capillary-like tubules were observed under a microscope (×100).

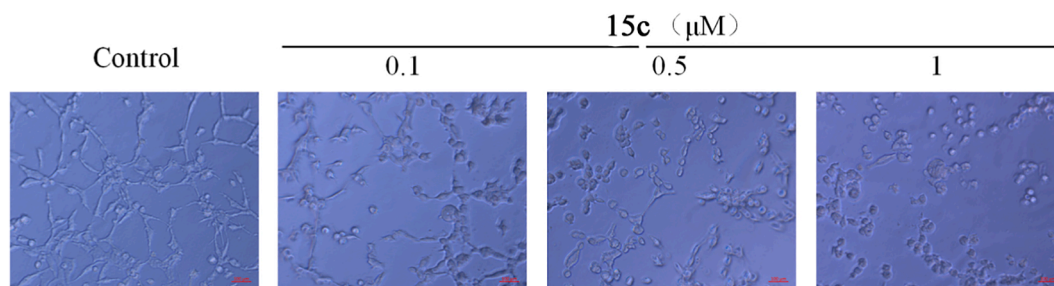


Fig. 11. Disruption of **15c** on newly formed vascular structures *in vitro*. Representative images of control vehicle or **15c** (0.1, 0.5 and 1 μM) treated HUVEC capillary-like tubular network ($\times 100$).

H_2O (50 mL), and the aqueous phase was extracted with ethyl acetate (3×50 mL). The combined organic extracts were dried over anhydrous Na_2SO_4 , filtered, and the solvent was evaporated *in vacuo*. The crude product was purified by column chromatography (PE: EA = 100:1 ~ 50:1) to provide **9** as white solid. Yield: 43.85 g (95%). ^1H NMR (600 MHz, CDCl_3) δ 7.73 (d, $J = 8.4$ Hz, 1H), 6.58 (d, $J = 8.4$ Hz, 1H), 3.93 (s, 3H).

4.1.2. 2-Chloro-6-methoxynicotinic aldehyde (**10**)

To a pre-cooled (-78 $^\circ\text{C}$) solution of **9** (10.00 g, 45.3 mmol) in anhydrous THF (50 mL), a solution of *n*-butyl lithium (2.5 M, 24.0 mL) was slowly dropped in efficient agitation under atmosphere of argon, and the reaction mixture was allowed to stir for another 1.5 h. Subsequently, *N,N*-dimethylformamide (7.0 mL, 90.0 mmol) was added portionwise and the resulting mixture was allowed to slowly warm up to room temperature and stirred for 6 h. Next, H_2O (20 mL) was added and the mixture was extracted with ethyl acetate (3×30 mL). The combined organic extracts were dried over Na_2SO_4 , filtered, and the solvent was evaporated *in vacuo*. The crude product was purified by column chromatography (PE: EA = 80:1 ~ 50:1) to give **10** as a light yellow solid. Yield: 4.89 g (63%). ^1H NMR (600 MHz, CDCl_3) δ 10.30 (s, 1H), 8.10 (d, $J = 8.4$ Hz, 1H), 6.75 (d, $J = 8.4$ Hz, 1H), 4.04 (s, 3H).

4.1.3. 6-Methoxy-1H-pyrazolo[3,4-*b*]pyridine (**11**)

A solution of **10** (4.50 g, 26.3 mmol) and hydrazine hydrate (20 mL) in H_2O (10 mL) was stirred for 5 h at 130 $^\circ\text{C}$. Next, the resulting mixture was cooled to room temperature, and extracted with ethyl acetate (3×10 mL). The combined organic extract was washed with saturated NaHCO_3 solution (15 mL), and dried over Na_2SO_4 , filtered, and the solvent was evaporated *in vacuo*. The crude product was purified by column chromatography (PE: EA = 50:1 ~ 30:1) to give **11** as a white solid. Yield: 2.30 g (58%). ^1H NMR (600 MHz, CDCl_3) δ 7.93 (s, 1H), 7.90 (d, $J = 9.0$ Hz, 1H), 6.63 (d, $J = 9.0$ Hz, 1H), 4.02 (s, 3H); MS (ESI) m/z 150.1 for $[\text{M}+\text{H}]^+$.

4.1.4. 3-Bromo-6-methoxy-1H-pyrazolo[3,4-*b*]pyridine (**12**)

To a pre-cooled (-30 $^\circ\text{C}$) solution of **11** (2.0 g, 13.4 mmol) in dichloromethane (20 mL), *N*-bromosuccinimide (2.38 g, 13.4 mmol) was slowly added in portions followed by further stirred for 30 min. The resulting mixture was warmed to room temperature, and added H_2O (10 mL). The aqueous phase was extracted with dichloromethane (2×10 mL), the combined organic phases were dried over anhydrous magnesium sulphate, filtered, and the solvent was evaporated *in vacuo*. The crude product was purified by column chromatography (PE: EA = 100:1 ~ 30:1) to get **12** light yellow solid. Yield: 1.56 g (51%); ^1H NMR (600 MHz, CDCl_3) δ 7.78 (d, $J = 9.0$ Hz, 1H), 6.68 (d, $J = 9.0$ Hz, 1H), 4.02 (s, 3H).

4.1.5. General procedures for preparation of compounds **13a-e**

A solution of **12** (1.50 g, 6.6 mmol) and sodium hydride (0.24 g, 9.9 mmol) in anhydrous DMF (5 mL) was stirred for 30 min at 0 $^\circ\text{C}$.

Subsequently, haloalkane (9.9 mmol) in anhydrous DMF (5 mL) was added dropwise. The cooling bath was removed and stirring was continued for 24 h at room temperature. The solvent was evaporated *in vacuo* and the residue was dissolved in ethyl acetate (30 mL). The solution was washed with a saturated solution of Na_2CO_3 , dried over anhydrous Na_2SO_4 , filtered, and the solvent was evaporated *in vacuo*. The residue was purified by column chromatography to obtain **13a-e**.

4.1.5.1. 3-Bromo-6-methoxy-1-methyl-1H-pyrazolo[3,4-*b*]pyridine (**13a**)

White solid; yield: 64%; ^1H NMR (600 MHz, CDCl_3) δ 7.72 (d, $J = 9.0$ Hz, 1H), 6.61 (d, $J = 9.0$ Hz, 1H), 4.02 (s, 3H), 4.01 (s, 3H); ^{13}C NMR (150 MHz, CDCl_3) δ 164.9, 149.6, 131.2, 118.9, 110.7, 107.8, 53.8, 33.8; HRMS (ESI) m/z calculated for $\text{C}_8\text{H}_9\text{BrN}_3\text{O}$ $[\text{M}+\text{H}]^+$ 241.9924, found 241.9916.

4.1.5.2. 3-Bromo-1-cyclopentyl-6-methoxy-1H-pyrazolo[3,4-*b*]pyridine (**13b**)

White solid; yield: 58%; ^1H NMR (600 MHz, CDCl_3) δ 7.70 (d, $J = 8.4$ Hz, 1H), 6.60 (d, $J = 8.4$ Hz, 1H), 5.26–5.20 (m, 1H), 4.01 (s, 3H), 2.17–2.13 (m, 4H), 2.01–1.96 (m, 2H), 1.73–1.69 (m, 2H); ^{13}C NMR (150 MHz, CDCl_3) δ 164.5, 149.1, 131.2, 118.5, 110.9, 107.7, 58.1, 53.8, 32.1 (2C), 24.7 (2C); HRMS (ESI) m/z calculated for $\text{C}_{12}\text{H}_{15}\text{BrN}_3\text{O}$ $[\text{M}+\text{H}]^+$ 296.0393, found 296.0387.

4.1.5.3. 3-Bromo-1-isopropyl-6-methoxy-1H-pyrazolo[3,4-*b*]pyridine (**13c**)

Light yellow solid; yield: 62%; ^1H NMR (600 MHz, CDCl_3) δ 7.71 (d, $J = 8.4$ Hz, 1H), 6.61 (d, $J = 8.4$ Hz, 1H), 5.13–5.08 (m, 1H), 4.01 (s, 3H), 1.57 (s, 3H), 1.56 (s, 3H); ^{13}C NMR (150 MHz, CDCl_3) δ 164.5, 148.6, 131.2, 118.6, 110.8, 107.7, 53.8, 49.2, 21.9 (2C); HRMS (ESI) m/z calculated for $\text{C}_{10}\text{H}_{13}\text{BrN}_3\text{O}$ $[\text{M}+\text{H}]^+$ 270.0237, found 270.0230.

4.1.5.4. 3-Bromo-6-methoxy-1-phenyl-1H-pyrazolo[3,4-*b*]pyridine (**13d**)

Light yellow solid; yield: 57%; ^1H NMR (600 MHz, CDCl_3) δ 8.26 (d, $J = 7.2$ Hz, 2H), 7.82 (d, $J = 9.0$ Hz, 1H), 7.53–7.52 (m, 1H), 7.51–7.49 (m, 2H), 6.74 (d, $J = 9.0$ Hz, 1H), 4.07 (s, 3H); ^{13}C NMR (150 MHz, CDCl_3) δ 164.0, 147.9, 138.1, 131.3, 130.6, 129.9, 127.9, 127.8, 124.9, 119.5, 111.4, 107.5, 53.1; HRMS (ESI) m/z calculated for $\text{C}_{13}\text{H}_{11}\text{BrN}_3\text{O}$ $[\text{M}+\text{H}]^+$ 304.0080, found 304.0081.

4.1.5.5. 1-Benzyl-3-bromo-6-methoxy-1H-pyrazolo[3,4-*b*]pyridine (**13e**)

Light yellow solid; yield: 66%; ^1H NMR (600 MHz, CDCl_3) δ 7.71 (d, $J = 9.0$ Hz, 1H), 7.38 (d, $J = 7.2$ Hz, 2H), 7.31–7.29 (m, 2H), 7.27–7.25 (m, 1H), 6.62 (d, $J = 8.4$ Hz, 1H), 5.54 (s, 2H), 4.02 (s, 3H); ^{13}C NMR (150 MHz, CDCl_3) δ 165.0, 149.4, 136.7, 131.3, 128.6 (2C), 128.2(2C), 127.8, 119.6, 110.8, 108.0, 53.9, 51.0; HRMS (ESI) m/z calculated for $\text{C}_{14}\text{H}_{12}\text{BrN}_3\text{NaO}$ $[\text{M}+\text{Na}]^+$ 340.0056, found 340.0050.

4.1.6. 3-Bromo-6-methoxy-1-(tetrahydro-2H-pyran-2-yl)-1H-pyrazolo[3,4-*b*]pyridine (**13f**)

To a solution of **12** (1.50 g, 6.6 mmol) and *p*-toluenesulfonic acid (0.23 g, 1.32 mmol) in anhydrous tetrahydrofuran (10 mL), 3,4-dihydro-2H-pyran (1.8 mL, 19.8 mmol) was slowly added under the atmosphere

of argon. The mixture was heated to reflux and stirring was continued for 3 h. The solvent was evaporated in vacuo and the residue, saturated NaHCO₃ solution (20 mL) was added, and the mixture was extracted with dichloromethane (3 × 20 mL). The combined organic extracts were dried over anhydrous Na₂SO₄, filtered, and the solvent was evaporated in vacuo. The residue was purified by column chromatography (PE: EA = 70:1 ~ 50:1) to obtain **13f** as white solid. Yield: 2.1 g (80%); ¹H NMR (600 MHz, CDCl₃) δ 7.73 (d, *J* = 8.4 Hz, 1H), 6.66 (d, *J* = 8.4 Hz, 1H), 5.94 (dd, *J* = 10.2, 2.4 Hz, 1H), 4.14–4.13 (m, 1H), 4.04 (s, 3H), 3.79–3.75 (m, 1H), 2.64–2.60 (m, 1H), 2.16–2.14 (m, 1H), 1.97–2.1.94 (m, 1H), 1.81–1.76 (m, 2H), 1.63–1.61 (m, 1H); ¹³C NMR (150 MHz, CDCl₃) δ 165.1, 149.6, 131.4, 121.5, 111.2, 108.5, 82.3, 67.9, 54.0, 29.4, 25.0, 23.0; HRMS (ESI) *m/z* calculated for C₁₂H₁₅BrN₃O₂ [M+H]⁺ 334.0162, found 334.0159.

4.1.7. General procedures for preparation of compounds **14a–f**

To a solution of 4,5-bisdiphenylphosphine-9,9-dimethylxanthene and Pd(OAc)₂ in dried 1,4-dioxane, a solution of 3,4,5-trimethoxyaniline in 1,4-dioxane was added, and the resulting mixture was heated under reflux for 5 min in the atmosphere of argon. Subsequently, respective of intermediate **13a–f** and cesium carbonate were added in sequence, and the resulting mixture was heated under reflux for 3 h. Next, the solvent was evaporated in vacuo, and the residue was purified by column chromatography to obtain the target compounds **14a–d** and the intermediates **14e,f**.

4.1.7.1. 6-Methoxy-1-methyl-N-(3,4,5-trimethoxyphenyl)-1H-pyrazolo[3,4-*b*]pyridin-3-amine (14a). White solid; yield: 64%; m.p.: 199–201 °C; HPLC purity: 96.44% (MeOH: H₂O = 85:15, 1.0 mL/min, *t_R* = 6.109 min); ¹H NMR (600 MHz, CDCl₃) δ 7.68 (d, *J* = 8.4 Hz, 1H), 6.53 (s, 2H), 6.45 (d, *J* = 8.4 Hz, 1H), 6.11 (brs, 1H), 4.02 (s, 3H), 3.94 (s, 3H), 3.82 (s, 9H); ¹³C NMR (150 MHz, CDCl₃) δ 164.5, 153.6, 149.5, 142.7, 138.8, 131.3 (2C), 104.7 (2C), 101.8, 94.6 (2C), 61.0, 55.9 (2C), 53.5, 33.1; MS (ESI) *m/z* 345.2 for [M+H]⁺; HRMS (ESI) *m/z* calculated for C₁₇H₂₁N₄O₄ [M+H]⁺ 345.1563, found 345.1568.

4.1.7.2. 1-Cyclopentyl-6-methoxy-N-(3,4,5-trimethoxyphenyl)-1H-pyrazolo[3,4-*b*]pyridin-3-amine (14b). White solid; yield: 75%; m.p.: 203–205 °C; HPLC purity: 97.23% (MeOH: H₂O = 85:15, 1.0 mL/min, *t_R* = 11.367 min); ¹H NMR (600 MHz, CDCl₃) δ 7.69 (d, *J* = 8.4 Hz, 1H), 6.66 (s, 2H), 6.45 (d, *J* = 8.4 Hz, 1H), 6.17 (brs, 1H), 5.25 (brs, 1H), 4.01 (s, 3H), 3.83 (s, 9H), 2.18–2.12 (m, 4H), 2.02–1.97 (m, 2H), 1.76–1.72 (m, 2H); ¹³C NMR (150 MHz, CDCl₃) δ 164.4, 153.5, 148.9, 142.5, 138.3, 131.7 (2C), 104.8 (2C), 101.5, 94.7 (2C), 61.0, 57.4, 55.6 (2C), 53.6, 31.8 (2C), 24.5 (2C); MS (ESI) *m/z* 399.2 for [M+H]⁺; HRMS (ESI) *m/z* calculated for C₂₁H₂₇N₄O₄ [M+H]⁺ 399.2032, found 399.2039.

4.1.7.3. 1-Isopropyl-6-methoxy-N-(3,4,5-trimethoxyphenyl)-1H-pyrazolo[3,4-*b*]pyridin-3-amine (14c). Yellow solid; yield: 66%; m.p.: 172–174 °C; HPLC purity: 96.30% (MeOH: H₂O = 85:15, 1.0 mL/min, *t_R* = 8.101 min); ¹H NMR (600 MHz, CDCl₃) δ 7.69 (d, *J* = 8.4 Hz, 1H), 6.63 (s, 2H), 6.46 (s, 1H), 6.13 (brs, 1H), 5.08 (brs, 1H), 4.01 (s, 3H), 3.83 (s, 9H), 1.55 (d, *J* = 6.6 Hz, 6H); ¹³C NMR (150 MHz, CDCl₃) δ 164.1, 153.4 (2C), 151.7, 149.2, 139.0, 136.6, 133.4, 106.4 (2C), 104.4, 102.4, 61.0, 56.2 (2C), 53.7, 49.8, 20.6 (2C); MS (ESI) *m/z* 373.2 for [M+H]⁺; HRMS (ESI) *m/z* calculated for C₁₉H₂₅N₄O₄ [M+H]⁺ 373.1876, found 373.1882.

4.1.7.4. 6-Methoxy-1-phenyl-N-(3,4,5-trimethoxyphenyl)-1H-pyrazolo[3,4-*b*]pyridin-3-amine (14d). Yellow solid; yield: 68%; m.p.: 189–191 °C; HPLC purity: 95.03% (MeOH: H₂O = 85:15, 1.0 mL/min, *t_R* = 8.854 min); ¹H NMR (600 MHz, CDCl₃) δ 8.35 (d, *J* = 9.0 Hz, 2H), 7.80 (d, *J* = 8.4 Hz, 1H), 7.48 (t, *J* = 8.4 Hz, 2H), 7.21 (t, *J* = 8.4 Hz, 1H), 6.85 (s, 2H), 6.58 (d, *J* = 8.4 Hz, 1H), 4.07 (s, 3H), 3.88 (s, 6H), 3.84 (s, 3H); ¹³C NMR (150 MHz, CDCl₃) δ 164.5, 153.4, 148.6, 144.3, 140.0, 137.8,

130.9, 128.8 (2C), 124.0 (2C), 119.0 (2C), 105.4 (2C), 104.0, 94.8 (2C), 61.0, 55.9 (2C), 53.8; MS (ESI) *m/z* 407.2 for [M+H]⁺; HRMS (ESI) *m/z* calculated for C₂₂H₂₃N₄O₄ [M+H]⁺ 407.1719, found 407.1728.

4.1.7.5. 1-Benzyl-6-methoxy-N-(3,4,5-trimethoxyphenyl)-1H-pyrazolo[3,4-*b*]pyridin-3-amine (14e). Yellow solid; yield: 61%; ¹H NMR (600 MHz, CDCl₃) δ 7.69 (d, *J* = 8.4 Hz, 1H), 7.38 (d, *J* = 7.2 Hz, 2H), 7.30 (t, *J* = 7.2 Hz, 2H), 6.56 (s, 2H), 6.48 (d, *J* = 8.4 Hz, 1H), 6.19 (brs, 1H), 5.48 (s, 2H), 4.03 (s, 3H), 3.80 (s, 3H), 3.76 (s, 6H); ¹³C NMR (150 MHz, CDCl₃) δ 164.8 (2C), 153.6 (2C), 149.5, 138.5, 137.4 (2C), 131.3 (2C), 128.5 (2C), 128.2, 127.6, 105.2 (2C), 94.8 (2C), 61.0, 55.9, 53.7, 50.0, 29.7; MS (ESI) *m/z* 421.2 for [M+H]⁺.

4.1.7.6. 6-Methoxy-1-(tetrahydro-2H-pyran-2-yl)-N-(3,4,5-trimethoxyphenyl)-1H-pyrazolo[3,4-*b*]pyridin-3-amine (14f). White solid; yield: 72%; ¹H NMR (600 MHz, CDCl₃) δ 7.66 (d, *J* = 8.4 Hz, 1H), 6.57 (s, 2H), 6.48 (d, *J* = 8.4 Hz, 1H), 6.23 (s, 1H), 5.93 (dd, *J* = 8.4, 2.4 Hz, 1H), 4.15 (d, *J* = 9.0 Hz, 1H), 4.03 (s, 3H), 3.82–3.78 (m, 10H), 2.61–2.59 (m, 1H), 2.17–2.15 (m, 1H), 2.02–1.99 (m, 1H), 1.87–1.75 (m, 2H), 1.64–1.62 (m, 1H); ¹³C NMR (150 MHz, CDCl₃) δ 164.6, 153.6, 149.9, 143.9, 138.4, 132.5, 131.4, 105.6 (2C), 102.7, 95.1 (2C), 81.7, 68.0, 61.0, 55.9 (2C), 53.6, 29.4, 25.2, 23.2; MS (ESI) *m/z* 415.2 for [M+H]⁺.

4.1.8. General procedures for preparation of compounds **15a,b**

To a pre-cooled (0 °C) solution of **14a,b** (0.8 mmol) in DMF (5 mL), sodium hydride (1.0 mmol) was slowly add, and the resulting mixture was stirred for 30 min at 0 °C. Subsequently, haloalkane (1.0 mmol) in anhydrous DMF (5 mL) was added dropwise, and the cooling bath was removed and stirring was continued for 24 h at room temperature. The solvent was evaporated in vacuo and H₂O (10 mL) was added. Next, the mixture was extracted with ethyl acetate (3 × 10 mL), and the combined organic extracts were dried over anhydrous Na₂SO₄, filtered, and the solvent was evaporated in vacuo. The residue was purified by column chromatography to give the corresponding product.

4.1.8.1. 6-Methoxy-N,1-dimethyl-N-(3,4,5-trimethoxyphenyl)-1H-pyrazolo[3,4-*b*]pyridin-3-amine (15a). White solid; yield: 51%; m.p.: 124–126 °C; HPLC purity: 96.31% (MeOH: H₂O = 85:15, 1.0 mL/min, *t_R* = 10.268 min); ¹H NMR (600 MHz, CDCl₃) δ 7.02 (d, *J* = 8.4 Hz, 1H), 6.40 (s, 2H), 6.25 (d, *J* = 8.4 Hz, 1H), 3.99 (s, 3H), 3.95 (s, 3H), 3.86 (s, 3H), 3.75 (s, 6H), 3.48 (s, 3H); ¹³C NMR (150 MHz, CDCl₃) δ 164.1, 153.6 (2C), 150.0, 147.6, 143.8, 134.4, 133.1 (2C), 104.0, 101.8, 100.2 (2C), 61.0, 56.1 (2C), 53.4, 40.3, 33.0; MS (ESI) *m/z* 359.2 for [M+H]⁺; HRMS (ESI) *m/z* calculated for C₁₈H₂₃N₄O₄ [M+H]⁺ 359.1719, found 359.1726.

4.1.8.2. N,1-Dicyclopentyl-6-methoxy-N-(3,4,5-trimethoxyphenyl)-1H-pyrazolo[3,4-*b*]pyridin-3-amine (15b). White solid; yield: 49%; m.p.: 111–113 °C; HPLC purity: 97.23% (MeOH: H₂O = 85:15, 1.0 mL/min, *t_R* = 11.506 min); ¹H NMR (600 MHz, CDCl₃) δ 6.71 (d, *J* = 8.4 Hz, 1H), 6.32 (s, 2H), 6.19 (d, *J* = 8.4 Hz, 1H), 5.21–5.18 (m, 1H), 4.53–4.50 (m, 1H), 3.96 (s, 3H), 3.86 (s, 3H), 3.75 (s, 6H), 2.15–2.11 (m, 6H), 2.02–1.18 (m, 4H) 1.71–1.62 (m, 6H); ¹³C NMR (150 MHz, CDCl₃) δ 163.6, 153.3 (2C), 149.3, 146.4 (2C), 135.1, 132.7 (2C), 104.1, 103.3 (2C), 61.3, 61.0, 57.0, 56.1 (2C), 53.4, 31.8 (2C), 29.9 (2C), 24.8 (2C), 23.5 (2C); MS (ESI) *m/z* 467.3 for [M+H]⁺; HRMS (ESI) *m/z* calculated for C₂₆H₃₅N₄O₄ [M+H]⁺ 467.2658, found 467.2668.

4.1.9. General procedures for preparation of compounds **15c–l**

The pre-cooled solution of **14f** (0.8 mmol) in DMF (5 mL) (0 °C) was treated with various haloalkane by similar procedure as description to synthesize **14a,b**. Then the obtained intermediate (0.6 mmol) was directly dissolved in ethanol (5 mL), and added concentrated hydrochloric acid (3 mL) at room temperature, and stirring was continued at room temperature for 24 h. The solvent was evaporated in vacuo and the

residue was dissolved in ethyl acetate (10 mL) and H₂O (5 mL). The organic layer was washed with a saturated solution of Na₂CO₃, dried over anhydrous Na₂SO₄, filtered, and the solvent of evaporated in vacuo. Next, the residue was purified by column chromatography to provide the corresponding target compounds **15c–l**.

4.1.9.1. 6-Methoxy-N-methyl-N-(3,4,5-trimethoxyphenyl)-1H-pyrazolo [3,4-b]pyridin-3-amine (15c). White solid; yield: 64%; m.p.: 159–161 °C; HPLC purity: 95.59% (MeOH: H₂O = 85:15, 1.0 mL/min, *t_R* = 5.182 min); ¹H NMR (600 MHz, CDCl₃) δ 7.03 (d, *J* = 8.4 Hz, 1H), 6.44 (s, 2H), 6.31 (d, *J* = 8.4 Hz, 1H), 3.99 (s, 3H), 3.87 (s, 3H), 3.77 (s, 6H), 3.50 (s, 3H); ¹³C NMR (150 MHz, CDCl₃) δ 164.0, 153.6 (2C), 150.3, 142.8, 132.1 (2C), 129.2, 108.0, 106.9, 104.2 (2C), 61.0, 56.3 (2C), 53.6, 33.6; MS (ESI) *m/z* 345.2 for [M+H]⁺; HRMS (ESI) *m/z* calculated for C₁₇H₂₁N₄O₄ [M+H]⁺ 345.1563, found 345.1570.

4.1.9.2. N-Ethyl-6-methoxy-N-(3,4,5-trimethoxyphenyl)-1H-pyrazolo [3,4-b]pyridin-3-amine (15d). Yellow solid; yield: 65%; m.p.: 137–139 °C; HPLC purity: 96.88% (MeOH: H₂O = 85:15, 1.0 mL/min, *t_R* = 5.476 min); ¹H NMR (600 MHz, CDCl₃) δ 6.91 (d, *J* = 8.4 Hz, 1H), 6.43 (s, 2H), 6.28 (d, *J* = 8.4 Hz, 1H), 3.99 (s, 3H), 3.96 (q, *J* = 7.2 Hz, 2H), 3.88 (s, 3H), 3.77 (s, 6H), 1.32 (t, *J* = 7.2 Hz, 3H); ¹³C NMR (150 MHz, CDCl₃) δ 164.4, 153.6 (2C), 151.7, 148.7, 142.0, 133.5, 104.6 (2C), 102.0 (2C), 61.0, 56.1 (2C), 53.8, 47.1, 12.9; MS (ESI) *m/z* 359.2 for [M+H]⁺; HRMS (ESI) *m/z* calculated for C₁₈H₂₃N₄O₄ [M+H]⁺ 359.1719, found 359.1727.

4.1.9.3. 6-Methoxy-N-propyl-N-(3,4,5-trimethoxyphenyl)-1H-pyrazolo [3,4-b]pyridin-3-amine (15e). Yellow solid; yield: 55%; m.p.: 140–142 °C; HPLC purity: 96.99% (MeOH: H₂O = 85:15, 1.0 mL/min, *t_R* = 5.952 min); ¹H NMR (600 MHz, CDCl₃) δ 6.93 (d, *J* = 8.4 Hz, 1H), 6.43 (s, 2H), 6.29 (d, *J* = 8.4 Hz, 1H), 4.02 (s, 3H), 3.88 (s, 3H), 3.84 (t, *J* = 6.6 Hz, 2H), 3.76 (s, 6H), 1.81–1.79 (m, 2H), 1.00 (t, *J* = 6.6 Hz, 3H); ¹³C NMR (150 MHz, CDCl₃) δ 164.4, 153.6, 151.7, 149.0, 142.5, 135.0, 133.5, 130.9, 128.8, 104.6, 101.9 (2C), 61.2, 56.1 (2C), 54.5, 53.7, 20.9, 11.5; MS (ESI) *m/z* 373.2 for [M+H]⁺; HRMS (ESI) *m/z* calculated for C₁₉H₂₅N₄O₄ [M+H]⁺ 373.1876, found 373.1883.

4.1.9.4. N-Isopropyl-6-methoxy-N-(3,4,5-trimethoxyphenyl)-1H-pyrazolo [3,4-b]pyridin-3-amine (15f). Light yellow solid; yield: 60%; m.p.: 110–112 °C; HPLC purity: 96.20% (MeOH: H₂O = 85:15, 1.0 mL/min, *t_R* = 5.650 min); ¹H NMR (600 MHz, CDCl₃) δ 6.48 (d, *J* = 9.0 Hz, 1H), 6.43 (s, 2H), 6.19 (d, *J* = 9.0 Hz, 1H), 4.68–4.66 (m, 1H), 3.95 (s, 3H), 3.91 (s, 3H), 3.78 (s, 6H), 1.29 (d, *J* = 6.6 Hz, 6H); ¹³C NMR (150 MHz, CDCl₃) δ 164.3, 153.4 (2C), 151.7, 149.4, 138.9, 133.4, 106.5 (2C), 104.5, 61.1, 56.2 (2C), 53.7, 49.7, 20.6 (2C); MS (ESI) *m/z* 373.2 for [M+H]⁺; HRMS (ESI) *m/z* calculated for C₁₉H₂₅N₄O₄ [M+H]⁺ 373.1876, found 373.1882.

4.1.9.5. N-(2-Fluoroethyl)-6-methoxy-N-(3,4,5-trimethoxyphenyl)-1H-pyrazolo[3,4-b]pyridin-3-amine (15g). White solid; yield: 63%; m.p.: 147–149 °C; HPLC purity: 95.79% (MeOH: H₂O = 85:15, 1.0 mL/min, *t_R* = 5.233 min); ¹H NMR (600 MHz, CDCl₃) δ 6.89 (d, *J* = 8.4 Hz, 1H), 6.52 (s, 2H), 6.28 (d, *J* = 8.4 Hz, 1H), 4.79 (t, *J* = 4.8 Hz, 1H), 4.71 (t, *J* = 4.8 Hz, 1H), 4.21 (t, *J* = 4.8 Hz, 1H), 4.16 (t, *J* = 4.8 Hz, 1H), 3.97 (s, 3H), 3.88 (s, 3H), 3.76 (s, 6H); ¹³C NMR (150 MHz, CDCl₃) δ 164.6, 153.7, 151.9, 148.3, 142.3, 135.6, 133.5, 130.9, 128.8, 104.9, 102.6, 101.6, 80.9, 65.5, 61.1, 56.1 (2C), 53.1; MS (ESI) *m/z* 377.3 for [M+H]⁺; HRMS (ESI) *m/z* calculated for C₁₈H₂₂N₄O₄ [M+H]⁺ 377.1625, found 377.1632.

4.1.9.6. N-(2,2-Difluoroethyl)-6-methoxy-N-(3,4,5-trimethoxyphenyl)-1H-pyrazolo [3,4-b]pyridin-3-amine (15h). White solid; yield: 56%; m.p.: 147–149 °C; HPLC purity: 98.03% (MeOH: H₂O = 85:15, 1.0 mL/min, *t_R* = 5.302 min); ¹H NMR (600 MHz, CDCl₃) δ 6.84 (d, *J* = 8.4 Hz,

1H), 6.51 (s, 2H), 6.30–6.28 (m, 2H), 4.21–4.15 (m, 2H), 3.99 (s, 3H), 3.89 (s, 3H), 3.77 (s, 6H); ¹³C NMR (150 MHz, CDCl₃) δ 164.7, 153.8 (2C), 151.8, 148.2, 141.9, 136.0, 114.0 (t, *J* = 241.5 Hz, 1C), 105.2, 102.8 (2C), 101.1, 65.5, 61.1, 56.2 (2C), 53.8; MS (ESI) *m/z* 395.2 for [M+H]⁺; HRMS (ESI) *m/z* calculated for C₁₈H₂₁F₂N₄O₄ [M+H]⁺ 395.1531, found 395.1537.

4.1.9.7. N-(cyclopropylmethyl)-6-methoxy-N-(3,4,5-trimethoxyphenyl)-1H-pyrazolo [3,4-b]pyridin-3-amine (15i). Light yellow solid; yield: 55%; m.p.: 118–120 °C; HPLC purity: 96.39% (MeOH: H₂O = 85:15, 1.0 mL/min, *t_R* = 5.908 min); ¹H NMR (600 MHz, CDCl₃) δ 6.88 (d, *J* = 8.4 Hz, 1H), 6.49 (s, 2H), 6.27 (d, *J* = 8.4 Hz, 1H), 3.99 (s, 3H), 3.89 (s, 3H), 3.77 (s, 6H), 3.74 (d, *J* = 6.6 Hz, 2H), 1.29–1.25 (m, 1H), 0.49 (d, *J* = 6.6 Hz, 2H), 0.24 (d, *J* = 6.6 Hz, 2H); ¹³C NMR (150 MHz, CDCl₃) δ 164.5, 153.6 (2C), 151.8, 149.2, 142.4, 133.5, 104.7 (2C), 102.8 (2C), 61.1, 57.1, 56.2 (2C), 53.7, 9.9, 3.9 (2C); MS (ESI) *m/z* 385.2 for [M+H]⁺; HRMS (ESI) *m/z* calculated for C₂₀H₂₅N₄O₄ [M+H]⁺ 385.1876, found 385.1882.

4.1.9.8. 6-Methoxy-N-(2-methoxyethyl)-N-(3,4,5-trimethoxyphenyl)-1H-pyrazolo [3,4-b]pyridin-3-amine (15j). White solid; yield: 52%; m.p.: 127–129 °C; HPLC purity: 97.55% (MeOH: H₂O = 85:15, 1.0 mL/min, *t_R* = 5.170 min); ¹H NMR (600 MHz, CDCl₃) δ 6.95 (d, *J* = 8.4 Hz, 1H), 6.55 (s, 2H), 6.29 (d, *J* = 8.4 Hz, 1H), 4.09 (t, *J* = 4.8 Hz, 2H), 4.01 (s, 3H), 3.88 (s, 3H), 3.76 (s, 9H), 3.72 (t, *J* = 4.8 Hz, 2H); ¹³C NMR (150 MHz, CDCl₃) δ 164.4, 153.5, 151.7, 148.4, 142.5, 133.6, 130.9, 128.8, 104.6, 102.0, 101.8, 65.5, 61.0, 58.9, 56.0 (2C), 53.8, 52.2; MS (ESI) *m/z* 389.2 for [M+H]⁺; HRMS (ESI) *m/z* calculated for C₁₉H₂₅N₄O₅ [M+H]⁺ 389.1825, found 389.1832.

4.1.9.9. N-Cyclopentyl-6-methoxy-N-(3,4,5-trimethoxyphenyl)-1H-pyrazolo[3,4-b]pyridin-3-amine (15k). White solid; yield: 56%; m.p.: 145–148 °C; HPLC purity: 95.27% (MeOH: H₂O = 85:15, 1.0 mL/min, *t_R* = 6.598 min); ¹H NMR (600 MHz, CDCl₃) δ 6.49 (d, *J* = 9.0 Hz, 1H), 6.45 (s, 2H), 6.22 (d, *J* = 9.0 Hz, 1H), 4.61–4.60 (m, 1H), 4.00 (s, 3H), 3.93 (s, 3H), 3.80 (s, 6H), 2.09–2.08 (m, 2H), 1.65–1.62 (m, 4H), 1.60–1.57 (m, 2H); ¹³C NMR (150 MHz, CDCl₃) δ 164.4, 153.4 (2C), 151.7, 150.0, 140.0, 133.3, 130.8, 128.8, 106.4, 104.7, 102.5, 61.1, 61.0, 56.2 (2C), 53.6, 29.7 (2C), 23.1 (2C); MS (ESI) *m/z* 399.3 for [M+H]⁺; HRMS (ESI) *m/z* calculated for C₂₁H₂₇N₄O₄ [M+H]⁺ 399.2032, found 399.2038.

4.1.9.10. N-Benzyl-6-methoxy-N-(3,4,5-trimethoxyphenyl)-1H-pyrazolo [3,4-b]pyridin-3-amine (15l). White solid; yield: 58%; m.p.: 167–169 °C; HPLC purity: 97.43% (MeOH: H₂O = 85:15, 1.0 mL/min, *t_R* = 6.255 min); ¹H NMR (600 MHz, CDCl₃) δ 7.38 (d, *J* = 6.6 Hz, 1H), 7.31–7.28 (m, 3H), 7.23 (d, *J* = 6.6 Hz, 1H), 7.07 (d, *J* = 8.4 Hz, 1H), 6.35 (s, 2H), 6.33 (d, *J* = 8.4 Hz, 1H), 5.16 (s, 2H), 3.98 (s, 3H), 3.84 (s, 3H), 3.66 (s, 6H); ¹³C NMR (150 MHz, CDCl₃) δ 164.5, 153.5 (2C), 151.7, 148.6, 142.5, 139.1, 133.4, 128.4 (2C), 127.5 (2C), 126.9 (2C), 105.0 (2C), 102.0, 100.7 (2C), 61.0, 56.2, 56.0, 53.8; MS (ESI) *m/z* 385.2 for [M+H]⁺; HRMS (ESI) *m/z* calculated for C₂₃H₂₅N₄O₄ [M+H]⁺ 421.1876, found 421.1883.

4.2. Biology

4.2.1. MTT assay

Cells grown in the logarithmic phase were seeded into 96-well plates (5 × 10³ cells/well) for 24 h, and then exposed to different concentrations of the test compounds for 72 h. After attached cells were incubated with 5 mg/mL MTT (Sigma, USA) for another 4 h, the suspension was discarded, and subsequently the dark blue crystals (formazan) were solubilized in dimethyl sulfoxide (DMSO). The absorbance of the solution at 490 nm was measured using a multifunction microplate reader (Molecular Devices, Flex Station 3), and each experiment was performed at least in triplicate. IC₅₀ values, which represent the drug

concentrations required to cause 50% cancer cell growth inhibition, were used to express the cytotoxic effects of each compound and were calculated with GraphPad Prism Software version 5.02 (GraphPad Inc., La Jolla, CA, USA).

4.2.2. *In vitro* tubulin polymerization assay

Pig brain microtubule protein was isolated by three cycles of temperature-dependent assembly/disassembly according to Shelanski et al in 100 mM PIPES (pH 6.5), 1 mM MgSO₄, 2 mM EGTA, 1 mM GTP and 1 mM 2-mercaptoethanol. In the first cycle of polymerization, glycerol and phenylmethylsulfonyl fluoride were added to 4 M and 0.2 mM, respectively. Homogeneous tubulin was prepared from microtubule protein by phosphocellulose (P11) chromatography. The purified proteins were stored in aliquots at -70 °C. Tubulin protein was mixed with different concentrations of compound in PEM buffer (100 mM PIPES, 1 mM MgCl₂, and 1 mM EGTA) containing 1 mM GTP and 5% glycerol. Microtubule polymerization was monitored at 37 °C by light scattering at 340 nm using a SPECTRA MAX 190 (Molecular Device) spectrophotometer. The plateau absorbance values were used for calculations.

4.2.3. Immunofluorescence microscopy

In a 10 mm confocal culture dish, 3 × 10⁴ cells were grown for 24 h and then incubated in the presence or absence of compound **15c** at the indicated concentrations for another 6 h. After being washed with phosphate-buffered solution (PBS) and fixed in 4% prewarmed (37 °C) paraformaldehyde for 15 min, the cells were permeabilized with 0.5% Triton X-100 for 15 min and blocked for 30 min in 10% goat serum. Then, the cells were incubated with mouse anti-tubulin antibody (CST, USA) at 4 °C overnight, washed with PBS three times, and incubated with goat antimouse IgG/Alexa-Fluor 488 antibody (Invitrogen, USA) for 1 h. The samples were immediately visualized on a Zeiss LSM 570 laser scanning confocal microscope (Carl Zeiss, Germany) after the nuclei were stained with DAPI (Solarbio, China) in the dark at room temperature for 10 min.

4.2.4. Cell cycle analysis

Cells were seeded in 6-well plates (3 × 10⁵ cells/well), incubated in the presence or absence of compound **15c** at the indicated concentrations for 24 h, harvested by centrifugation, and then fixed in ice-cold 70% ethanol overnight. After the ethanol was removed the next day, the cells were resuspended in ice-cold PBS, treated with RNase A (Keygen Biotech, China) at 37 °C for 30 min, and then incubated with the DNA staining solution propidium iodide (PI, Keygen Biotech, China) at 4 °C for 30 min. Approximately 10 000 events were detected by flow cytometry (Beckman Coulter, Epics XL) at 488 nm.

4.2.5. Western blot analysis

MCF-7 or HUVEC cells (5.0 × 10⁵ cells/dish) were incubated with or without **15c** at various concentrations for 6 h. After incubation, the cells were collected by centrifugation and washed twice with phosphate-buffered saline chilled to 0 °C. Then, the cells were homogenized in RIPA lysis buffer containing 150 mM NaCl, 50 mM Tris (pH 7.4), 1% (w/v) sodium deoxycholate, 1% (v/v) Triton X-100, 0.1% (w/v) SDS, and 1 mM EDTA (Beyotime, China). The lysates were incubated on ice for 30 min, intermittently vortexed every 5 min, and centrifuged at 12,500 g for 15 min to harvest the supernatants. Next, the protein concentrations were determined by a BCA Protein Assay Kit (Thermo Fisher Scientific, Rockford, Illinois, USA). The protein extracts were reconstituted in loading buffer containing 62 mM Tris-HCl, 2% SDS, 10% glycerol, and 5% β-mercaptoethanol (Beyotime, China), and the mixture was boiled at 100 °C for 10 min. An equal amount of the proteins (50 mg) was separated by 8–12% sodium dodecyl sulfate-polyacrylamide gel electrophoresis (SDS-PAGE) and transferred to nitrocellulose membranes (Amersham Biosciences, Little Chalfont, Buckinghamshire, UK). Then, the membranes were blocked with 5% nonfat dried milk in TBS containing 1% Tween-20 for 90 min at room temperature and were

incubated overnight with specific primary antibodies (CST, USA) at 4 °C. After three washes in TBST, the membranes were incubated with the appropriate HRP-conjugated secondary antibodies at room temperature for 2 h. The blots were developed with enhanced chemiluminescence (Pierce, Rockford, Illinois, USA) and were detected by an LAS4000 imager (GE Healthcare, Waukesha, Wisconsin, USA).

4.2.6. Wound healing assay

MCF-7 cells (5 × 10⁵ cells/well) were grown in petridishes for 24 h. Scratches were made in confluent monolayers using 200 μL pipette tip. Then, wounds were washed twice with PBS to remove non-adherent cell debris. The media containing different concentrations of the compound **15c** were added to the petridishes. Cells which migrated across the wound area were photographed under the phase contrast microscope (Nikon) after 0, 12 and 24 h treatment. The number of cells migrated in to the wound area was counted manually.

4.2.7. Transwell invasion assay

The Transwell (12 μm, Corning Incorporated) was pre-coated with 70 μL Matrigel for 5 h at 37 °C to achieve solidification. MCF-7 cells were harvested and resuspended in serum-free medium containing 0, 0.05, 0.1, 0.5 and 1 μM of compound **15c** and added into the upper wells of the Transwell chamber at the density of 5 × 10⁵ cells/mL. While 600 μL of ECM containing 10% FBS was added into the lower chambers which had been coated with 70 μL of Matrigel (1:8 dilution in serum-free medium, Corning/BD Biosciences). After 24 h of incubation at 37 °C, the invasion cells were fixed with methanol and stained with 0.1% crystal violet for 30 min, respectively. Then, the chambers were washed with PBS and left to dry. Images were photographed using an inverted fluorescence microscope (Zeiss, VERT1, USA) and counted by Image J software for three independent fields randomly.

4.2.8. Tubule formation assay

The Matrigel was slowly driven into the pre-cooled 96-well plate with a pre-cooled pipette tip. Wrap the 96-well plate with plastic wrap and put it in a 4 °C refrigerator. After the matrigel is covered with the bottom of the well and stabilized, place the 96-well plate in a 37 °C cell incubator and polymerize for 30 min. The digested HUVEC cells were resuspended in ECM medium containing 20% FBS, and HUVEC cells were seeded in 96-well plates at 5 × 10⁴ cells per well using a cell counting plate. Then add **15c** of different concentration for 6 h. After 6 h, observe the formation of cell tubules and take pictures under an inverted microscope.

To examine neovessel disruption, the formed capillary-like structures were exposed to serum-free culture DMEM medium with either vehicle or **15c** (0.1, 0.5 and 1 μM). After incubation for 6 h, photographs were taken. The number of left tubes was quantified and the disruption of neovasculature networks was expressed as [1-(tubes_{treated}/tubes_{vehicle})] × 100%.

4.2.9. Molecular docking

In this study, the tubulin structure was downloaded from the Protein Data Bank (PDB code 1SA0). Using Schrodinger software prepared the protein by removing of Mg²⁺, water molecules and colchicine. Then the ligand **15c** was minimized, and the docking procedure was performed by employing docking program in schrodinger software, and the structural image was obtained using PyMOL software.

4.3. Statistical analysis

All data in this study were obtained from three independent experiments and then expressed as the means ± SD. Statistically significant differences were assessed via SPSS 18.0 software (SPSS, IL, USA). A value of *p* < 0.05 was considered statistically significant.

Declaration of Competing Interest

The authors declare that they have no known competing financial interests or personal relationships that could have appeared to influence the work reported in this paper.

Acknowledgments

This work was financially supported by the National Natural Sciences Foundations of China (21672093).

Appendix A. Supplementary material

Supplementary data to this article can be found online at <https://doi.org/10.1016/j.bmc.2020.115985>.

References

- Jordan MA, Wilson L. Microtubules as a target for anti-cancer drugs. *Nat Rev Cancer*. 2004;4:253–265.
- Downing KH, Nogales E. Tubulin and microtubule structure. *Curr Opin Cell Biol*. 1998;10:16–22.
- Prota AE, Bargsten K, Zurwerra D, et al. Molecular mechanism of action of microtubule-stabilizing anticancer agents. *Science*. 2013;339:587–590.
- Kavallaris M. Microtubules and resistance to tubulin-binding agents. *Nat Rev Cancer*. 2010;10:194–204.
- Naaz F, Haider MR, Shafi S, et al. Anti-tubulin agents of natural origin: targeting taxol, vinca, and colchicine binding domains. *Eur J Med Chem*. 2019;171:310–331.
- Charles D, Mary AJ. Microtubule-binding agents: a dynamic field of cancer therapeutics. *Nat Rev Drug Discov*. 2010;9:790–803.
- Dark GG, Hill SA, Prise VE, et al. Combretastatin A-4, an agent that displays potent and selective toxicity toward tumor vasculature. *Cancer Res*. 1997;57:1829–1834.
- Tron GC, Pirali T, Sorba GF, et al. Medicinal chemistry of combretastatin A4: present and future directions. *J Med Chem*. 2006;49:3033–3044.
- Nagaiah G, Remick SC. Combretastatin A4 phosphate: a novel vascular disrupting agent. *Future Oncol*. 2010;6:1219–1228.
- Shreeves G, Poupard L, Zweifel M, et al. Phase II trial of combretastatin A4 phosphate, carboplatin, and paclitaxel in patients with platinum-resistant ovarian cancer. *Ann Oncol*. 2011;22:2036–2041.
- Anurag C, Pandeya SN, Kumar P, et al. Combretastatin A-4 analogs as anticancer agents. *Mini-Rev Med Chem*. 2007;7:1186–1205.
- Malebari AM, Greene LM, Nathwani SM, et al. β -Lactam analogues of combretastatin A-4 prevent metabolic inactivation by glucuronidation in chemoresistant HT-29 colon cancer cells. *Eur J Med Chem*. 2017;130:261–285.
- Chernysheva NB, Maksimenko AS, Andreyanov FA, et al. Regioselective synthesis of 3,4-diaryl-5-unsubstituted isoxazoles, analogues of natural cytostatic combretastatin A4. *Eur J Med Chem*. 2018;146:511–518.
- Kumar B, Sharma P, Gupta VP, et al. Synthesis and biological evaluation of pyrimidine bridged combretastatin derivatives as potential anticancer agents and mechanistic studies. *Bioorg Chem*. 2018;78:130–140.
- Nowikow C, Fuerster R, Kauderer M, et al. Synthesis and biological evaluation of cis-restrained carbocyclic combretastatin A-4 analogs: Influence of the ring size and saturation on cytotoxic properties. *Bioorg Med Chem*. 2019;27, 115032.
- Kong Y, Smith J, Li K, et al. Development of a novel near-infrared fluorescent theranostic combretastatin A-4 analogue, YK-5-252, to target triple negative breast cancer. *Bioorg Med Chem*. 2017;25:2226–2233.
- Sharma S, Poliks B, Chiauzzi C, et al. Characterization of the colchicine binding site on avian tubulin isotype β VI. *Biochemistry*. 2010;49:2932–2942.
- Bai R, Covell DG, Pei XF, et al. Mapping the binding site of colchicinoids on β -tubulin 2-chloroacetyl-2-demethylthiocolchicine covalently reacts predominantly with cysteine 239 and secondarily with cysteine 354. *J Biol Chem*. 2000;275:40443–40452.
- Romagnoli R, Baraldi PG, Sarkar T, et al. Synthesis and biological evaluation of 1-methyl-2-(3',4',5'-trimethoxybenzoyl)-3-aminoindoles as a new class of antimitotic agents and tubulin inhibitors. *J Med Chem*. 2008;51:1464–1468.
- Romagnoli R, Baraldi PG, Salvador MK, et al. Design, synthesis, in vitro, and in vivo anticancer and antiangiogenic activity of novel 3-arylamino benzofuran derivatives targeting the colchicine site on tubulin. *J Med Chem*. 2015;58:3209–3222.
- Tung YS, Coumar MS, Wu YS, et al. Scaffold-hopping strategy: synthesis and biological evaluation of 5,6-fused bicyclic heteroaromatics to identify orally bioavailable anticancer agents. *J Med Chem*. 2011;54:3076–3080.
- Mishra SS, Singh P. Hybrids molecules: the privileged scaffolds for various pharmaceuticals. *Eur J Med Chem*. 2016;124:500–536.
- Qi Z-Y, Hao S-Y, Tian H-Z, et al. Synthesis and biological evaluation of 1-(benzofuran-3-yl)-4-(3,4,5-trimethoxyphenyl)-1H-1,2,3-triazole derivatives as tubulin polymerization inhibitors. *Bioorg Chem*. 2020;94, 103392.
- Sang C-Y, Qin W-W, Zhang X-J, et al. Synthesis and identification of 2,4-bis(aminopyrimidines bearing 2,2,6,6-tetramethylpiperidine-N-oxyl as potential Aurora A inhibitors. *Bioorg Med Chem*. 2019;27:65–78.
- Gigant B, Wang C, Ravelli RBG, et al. Structural basis for the regulation of tubulin by vinblastine. *Nature*. 2005;435:519–522.
- Clarke PR, Allan LA. Cell-cycle control in the face of damage—a matter of life or death. *Trends Cell Biol*. 2009;19:89–98.
- Jackman M, Lindon C, Nigg EA, et al. Active cyclin B1-Cdk1 first appears on centrosomes in prophase. *Nat Cell Biol*. 2003;5:143–148.
- Sitohy B, Chang S, Sciuto TE, et al. Early actions of anti-vascular endothelial growth factor/vascular endothelial growth factor receptor drugs on angiogenic blood vessels. *Am J Pathol*. 2017;187:2337–2347.
- Li T, Kang G, Wang T, et al. Tumor angiogenesis and anti-angiogenic gene therapy for cancer. *Oncol Lett*. 2018;16:687–702.
- Xiang R, Guan X-W, Hui L, et al. Investigation of the anti-angiogenesis effects induced by deoxy podophyllotoxin-5-FU conjugate C069 against HUVE cells. *Bioorg Med Chem Lett*. 2017;27:713–717.
- Ahmed B, van Eijk LI, Bouma-Ter Steege JCA, et al. Vascular targeting effect of combretastatin A-4 phosphate dominates the inherent angiogenesis inhibitory activity. *Int J Cancer*. 2003;105:20–25.
- Mondal S, Adhikari N, Banerjee S, et al. Matrix metalloproteinase-9 (MMP-9) and its inhibitors in cancer: a minireview. *Eur J Med Chem*. 2020;194, 112260.
- Rundhaug JE. Matrix metalloproteinases and angiogenesis. *J Cell Mol Med*. 2005;9:267–285.
- Ruoslahti E. Specialization of tumour vasculature. *Nat Rev*. 2002;2:83–90.
- Porcù E, Salvador A, Primac I, et al. Vascular disrupting activity of combretastatin analogues. *Vasc Pharmacol*. 2016;83:78–89.